ACS APPLIED MATERIALS & INTERFACES

www.acsami.org

Research Article

Bubble Printing of Layered Silicates: Surface Chemistry Effects and Picomolar Förster Resonance Energy Transfer Sensing

Marcel Herber,[⊥] Ana Jiménez Amaya,[⊥] Nicklas Giese, Bharath Bangalore Rajeeva, Yuebing Zheng,* and Eric H. Hill*

Cite This: *ACS Appl. Mater. Interfaces* 2023, 15, 55022−55029

Read Online

ACCESS | Metrics & More | Article Recommendations | Supporting Information

ABSTRACT: The assembly of nanoparticles on surfaces in defined patterns has long been achieved via template-assisted methods that involve long deposition and drying steps and the need for molds or masks to obtain the desired patterns. Control over deposition of materials on surfaces via laser-directed microbubbles is a nascent technique that holds promise for rapid fabrication of devices down to the micrometer scale. However, the influence of surface chemistry on the resulting assembly using such approaches has so far not been studied. Herein, the printing of layered silicate nanoclays using a laser-directed microbubble was established. Significant differences in the macroscale structure of the printed patterns were observed for hydrophilic, pristine layered silicates compared to hydrophobic, modified layered silicates, which provided the first example of how the surface chemistry of such nanoscale objects results in changes in assembly with this approach. Furthermore, the ability of layered silicates to adsorb molecules at the interface was retained, which allowed the fabrication of proof-of-concept sensors based on Förster resonance energy transfer (FRET) from quantum dots embedded in the assemblies to bound dye molecules. The detection limit for Rhodamine 800 sensing via FRET was found to be on the order of 10^{-12} M, suggesting signal enhancement due to favorable interactions between the dye and nanoclay. This work sets the stage for future advances in the control of hierarchical assembly of nanoparticles by modification of surface chemistry while also demonstrating a quick and versatile approach to achieve ultrasensitive molecular sensors.

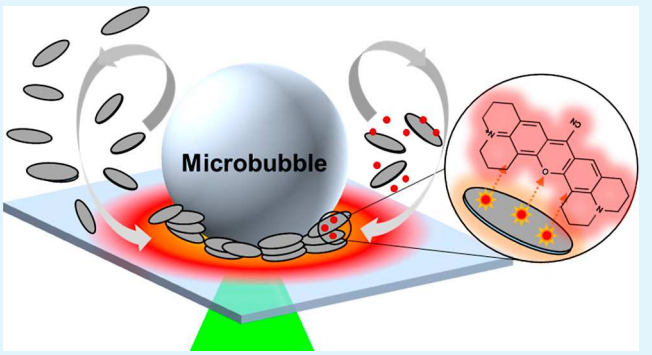

KEYWORDS: *bubble printing, bubble-pen lithography, microbubbles, nanoparticle assembly, Förster resonance energy transfer, laponite*

INTRODUCTION

The patterning of colloidal particles on surfaces by optically controlled microbubbles is a recent and nascent technique which holds promise for various applications.[1−4] The heating of metal nanostructures on a substrate with a focused laser can lead to relatively strong thermal gradients with low optical power, and with enough power, the formation of a microbubble due to solvent vaporization.[5−7] This thermal gradient can drag colloidal particles toward the substrate, while the stress tension gradient at the bubble interface leads to Marangoni convection, driving particles toward the microbubble. Particles bound to the bubble interface can then be immobilized at the substrate interface via hydrophobic interactions upon contact with the triple-contact line. Applications such as particle trapping,[8] plasmofluidic lenses,[9] and photothermal motors[10] have been enabled by such microbubbles. Furthermore, bubble-pen lithography or bubble printing (BP) has been applied in numerous ways, including patterning of semiconductor quantum dots (QDs),[11] fabrication of uniform Ag rings,[12] site-specific formation of Rh−Au alloys,[13] catalysts,[14] and deposition of conductive patterns composed of conductive polymers or sintered metallic nanoparticles.[15−17]

Hierarchical assembly is the process of small components coming together to form larger building blocks, which, in turn, can be used to build a larger superstructure with functional properties imparted by the building blocks used. There has been much recent interest in controlling the hierarchical assembly of functional nanoparticles to form ordered assemblies that span multiple length scales from the nano- to the macro-scale. However, there are challenges in the fabrication of such materials due to limitations in the methods used. Currently, most approaches involve casting, filtration, spin-coating, or layer-by-layer approaches to achieve both hierarchical assembly and the desired layered structure.

Received: July 6, 2023
Revised: October 7, 2023
Accepted: October 31, 2023
Published: November 15, 2023

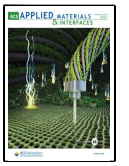

https://doi.org/10.1021/acsami.3c09760
ACS Appl. Mater. Interfaces 2023, 15, 55022−55029

Though these methods are easily scalable, they are also time-consuming and require large amounts of material. Furthermore, there is no current method to produce such materials in a site-specific manner; i.e., the patterning or controlled deposition of such materials into specific regions has not been achieved. Self-assembly of nanoparticles into supercrystals, field-assisted methods, and 3D-printing have all been recently studied toward hierarchical assembly of robust functional materials for device-oriented applications, as discussed in a recent review.[18]

While supercrystal assembly and 3D-printing methods are currently at an advanced stage of understanding, field-assisted assembly of hierarchical composite materials is currently at a nascent stage of research.[19] BP has already shown potential for hierarchical assembly of polystyrene spheres,[1] metal nanoparticles,[20] and MXenes,[21] all of which are of great interest for the development of functional materials. However, direct methods using optical printing have only recently been explored for hierarchical assembly, and control over anisotropic particle orientation during optically directed self-assembly has not yet been achieved.[19] The use of BP for directing assembly at the bubble interface would provide multiple advantages over the current fabrication methods for hierarchically assembled layered materials. First and foremost, directed assembly at the bubble interface allows near-instantaneous fabrication, removing the tedium of long casting times or complicated sequential processes needed for layer-by-layer or spin-coating methods. Second, the amount of material needed is very small as Marangoni convection drives particles to the interface from dispersion, increasing the local concentration of particles at the bubble interface. Finally, the particle assembly is directed by the movement of a laser, which can be programmed for the formation of arbitrary patterns.

Layered silicates are clay-like materials which are composed of an octahedral layer sandwiched between two tetrahedral silicate layers, with a thickness of ∼0.92 nm and diameters ranging from 25 nm to 5 μm, where the isomorphic substitution of interlayer ions leads to anionic basal surfaces.[22] This gives a high cation exchange capacity which has been used to modify the basal surfaces via electrostatic interactions,[23−29] whereas edge-modification strategies are also possible due to the Si−OH edge groups.[30−33] Herein, assemblies of the synthetic layered silicate Laponite (Lap) with different surface modifications were printed using BP. The aim of this study was twofold. First, layered silicates can serve as flexible platforms for a variety of applications, including sensors,[34−36] tissue engineering/wound healing,[37−41] biomaterials,[42,43] and drug delivery,[44−46] and the retention of the normal function of these materials after printing is paramount. Second, knowledge of how the surface chemistry of a well-defined anisotropic particle could influence the assembly is useful for achieving greater control over the final assembly geometry via particle surface chemistry.

METHODS

Laponite-RD (Lap-RD) and Laponite-EP (Lap-EP), which are pristine and organically modified nanoclays, respectively, were generously donated by BYK Additives. The Rhodamines 6G, B, and 101, obtained from Acros Organics, and Rhodamine 800 (R800) obtained from TCI were dissolved in water prior to use. CdSe/CdS core/shell QDs with emissions centered at 535, 590, and 625 nm were synthesized by the method of Yu and co-workers,[47] including surface modification with block copolymer poly(maleic anhydride-*alt*-1-octadecene)-40 kDa-polyethylene glycol-6 kDa and transfer to an aqueous dispersion;[11] QD concentrations (535 nm −1.75 μM; 590 nm −4.0 μM; 625 nm −0.2 μM) were determined using previously reported extinction coefficients.[48] Amine-terminated CdSe/ZnS QDs with an emission at 620 nm used for determining Förster resonance energy transfer (FRET) sensitivity were obtained from Sigma-Aldrich. Millipore-filtered water with a resistivity of 18.2 MΩ·cm was used in all cases.

The plasmonic gold nanoisland (AuNI) substrates were fabricated by depositing a 4 nm Au film on a glass coverslip with thermal deposition (Denton Vacuum, Moorestown, NJ) at a base pressure of 9×10^{-6} Torr, followed by thermal annealing at 550 °C for 2 h. The optical setup used for printing and spectroscopy consisted of an inverted optical microscope (Nikon Ti/Ti2) coupled to a 532 nm CW laser (Torus 532, Laser Quantum, Stockport, UK) that was passed through a 5× beam expander to fill the back of the microscope objective (100×, NA = 1.3, Plan Fluor, Nikon). Further details of the optical setup are given in Figure 1a, where the flow conditions and

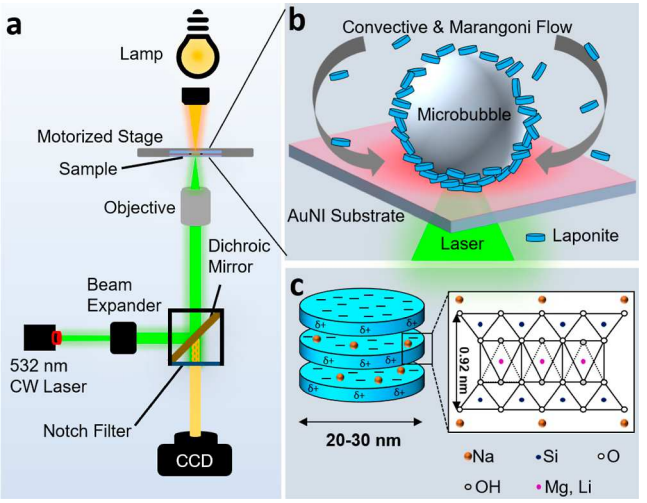

Figure 1. (a) Scheme of optical setup; (b) detail of BP process; and (c) depiction of the Lap structure.

structure of Lap are given in Figure 1b,c, respectively. Lap-RD and Lap-EP were dispersed in water with stirring overnight at concentrations of 10 mg/mL. The structure of the printed patterns was characterized by scanning electron microscopy (SEM) (FEI Quanta 3D FEG, FEI Company, Hillsboro, OR) operating at an acceleration voltage of 10−20 kV with gold coating and 3 kV without. For height measurements, printed lines were measured with an atomic force microscope (JPK NanoWizard 4XP, Bruker, Billerica, MA) with a PPP-NCHR tip with a tip diameter of 10 nm (Nanosensors, Neuchâtel, Switzerland). AFM measurements were recorded in Quantitative Imaging mode at a force of approximately 50−150 nN.

Printed patterns containing Lap-RD and QDs were prepared by first mixing 5 mL of Lap-RD (5 mg/mL) with 200 μL of QD dispersion, followed by sonication for 1 min and stirring for 10 min, and then BP as described. Emission spectra of printed patterns of Lap-RD with three different emission wavelengths of QDs were recorded with a spectrograph (Andor Shamrock 303i grating: 1199 L/mm; slit width: 45 μm) and an EMCCD (Andor Newton 970) integrated with the inverted microscope; signal was collected for 0.1 s using a 532 mW CW laser at 0.2 mW. Hybrid clay/QD patterns were printed from Lap-RD or Lap-EP (90 μL, 5 mg/mL) mixed with 620 nm emitting QDs (10 μL, 0.21 μM). In order to determine the sensitivity of hybrid clay/QD patterns, these were soaked in a series of R800 solutions with concentrations from 1 pM to 10 μM for 1 h, followed by drying under a stream of compressed air. Fluorescence measurements for FRET studies were carried out using a spectrograph (Andor Kymera 328i grating: 150 L/mm, 500 nm blaze; slit width: 20 μm) and EMCCD (Andor Newton 970); signal was collected through the microscope objective (60×, NA = 0.85, Plan Fluor, Nikon) for 0.05 s

https://doi.org/10.1021/acsami.3c09760
ACS Appl. Mater. Interfaces 2023, 15, 55022−55029

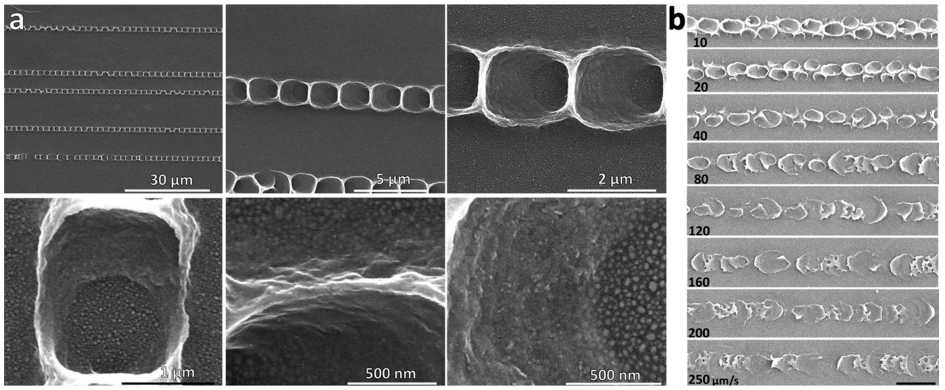

Figure 2. (a) Scanning electron micrographs of microstructures produced by BP of Lap-RD at different magnifications and (b) with different speeds of the heating laser movement. The AuNI substrate can be clearly observed as small islands in the bottom left and bottom right panels of (a).

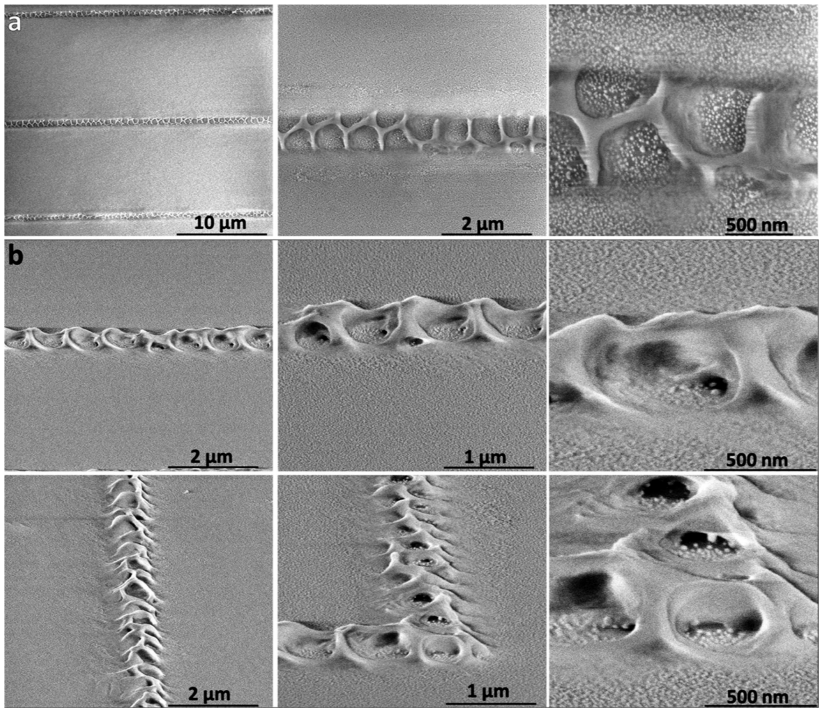

Figure 3. Scanning electron micrographs of printed Lap-EP (a) without tilt; (b) with 70° tilt.

with excitation by the 532 nm CW laser at 0.2 mW. To account for the differences between samples, fluorescence measurements were taken in a minimum of 5 different random printed regions for each concentration on the sample, with 3 samples for each clay type. Fluorescence microscopy images of QD/dye experiments were acquired by using a white excitation source with a Texas Red filter cube (Nikon).

RESULTS AND DISCUSSION

A microbubble is formed on the plasmonic substrate upon irradiation with a laser beam due to the plasmon-enhanced photothermal heating of the solvent. Marangoni convection then leads to the dragging of colloidal particles toward the microbubble, where they are then trapped at the interface between the bubble and the solvent, and finally immobilized on the substrate at the triple-contact line via noncovalent interactions.[1] Monneret et al. reported that at 100 °C in water, microbubbles are not expected because of a small radius of bubble curvature, which increases the boiling point. Thus, supercritical liquid water was observed before bubble formation to have a temperature of up to 220 °C.[5] CFD simulations showed that a temperature difference from the bottom to the top of a laser-induced microbubble resulted in a surface tension gradient. The flow velocity decreases with increasing distance from the bubble, changing from 100 to 1 μm/s at distances of 5 to 15 μm, respectively. This is reflected in the observed particle velocities; as the particle moves closer to the microbubble, the trapping speed increases drastically.[1]

A number of interesting preliminary observations were made. First, the presence of clay in an aqueous suspension increases the minimum power required for the formation of bubbles at the AuNI interface by 532 nm laser irradiation (1.5 vs 2.2 mW). Furthermore, interesting 3D structures were observed that likely arose due to particle assembly at the bubble interface, revealing the shape of the bubble before it dissipated or moved with the laser. In most previous studies of BP, a spot or ring of material is deposited radially without

https://doi.org/10.1021/acsami.3c09760
ACS Appl. Mater. Interfaces 2023, 15, 55022−55029

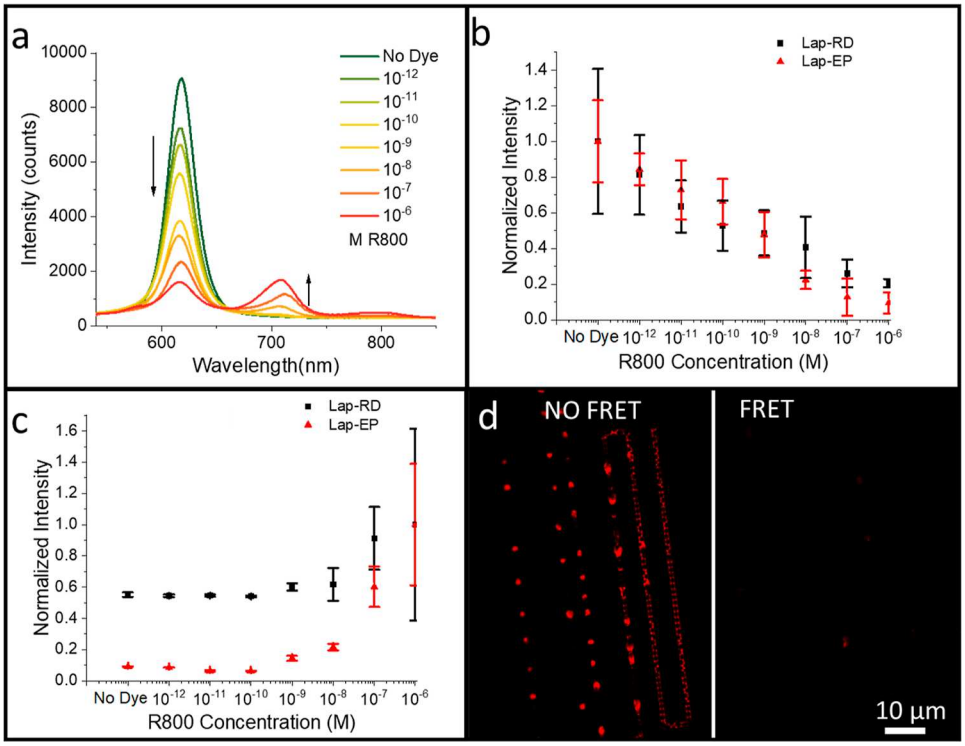

Figure 4. Hybrid Lap-QD microstructures: (a) fluorescence emission spectra collected on Lap-RD patterns printed with 620 nm emitting QDs after soaking in different concentrations of R800; (b) normalized fluorescence emission of Lap/QD micropatterns at 620 and (c) 704 nm; excitation by 532 nm laser at 0.2 mW for 0.05 s. (d) Fluorescence microscopy image of Lap-RD/QD micropatterns before (left panel) and after immersion in 10 μM R800 (right panel).

further variations in structure. Interestingly, the surface of the deposited structures has a texture of small features on the order of 20−30 nm, which is the lateral diameter of the layered silicate particles (Figure 2a, bottom right). This suggests that there may be some assembly of the clay particles at the bubble interface prior to the deposition of the material at the AuNI surface. Indeed, there have been previous reports of "armored bubbles" stabilizing foams and emulsions due to the self-assembly of layered silicate particles at the air−liquid interface of the bubble.[49,50] This interfacial assembly is also evident in the good gas-barrier properties of clay/polymer nanocomposites.[51] Further evidence of this could be observed when such long-lasting bubbles formed by BP at higher clay concentrations (4 mg/mL) were able to be trapped and manipulated to push other stationary bubbles by the heating laser through a combination of thermophoresis[52] and scattering forces (Video S1).

It was observed that the bubbles and resulting deposited structures were highly dependent on the speed of the laser (Figure 2b). While slower speeds (10−40 μm/s) led to quasi-toroidal patterns with clearly defined edges, speeds at 80 μm/s and above resulted in "smearing" of the printed assembly. This supports that the observed structure is indicative of interfacial assembly at the bubble interface and that increased speed of the laser movement leads to more dragging of the bubble, which then deposits the clay bound at the liquid−vapor interface onto the surface.

Influence of Surface Chemistry on Printing. To study how surface modification of the clay can influence the printing process, Lap-EP, which is modified along the edges with a hydrophobic polymer, was printed under conditions similar to those of Lap. Interestingly, it was observed that bubble-formed patterns of Lap-EP give a drastically different appearance upon deposition, in which the formation of sidewalls is reduced, and the appearance of one or more lines of deposited matter along the median of the printed pattern was observed (Figure 3, Video S2). The lack of sidewalls in the structure in the case of printed assemblies of Lap-EP, as opposed to the well-defined sidewalls in Lap-RD, suggests that the increased hydrophobicity of Lap-EP as opposed to that of pristine Lap-RD leads to a reduced preference for the clay to be exposed to the aqueous medium. In the case of Lap-EP, patterns clearly tend to reduce the area exposed to the aqueous medium and "open" entirely toward the exterior of the patterns. It is suspected that immediately upon the adsorption of Lap-EP at the bubble interface, the bubbles partition toward either side of the accumulating matter, in order to minimize free energy by reducing the interaction between Lap-EP and water, favoring interaction between Lap-EP and the vapor bubble. This can be somewhat observed via dark-field illumination during printing (Video S3). This is supported by SEM images taken with 70° tilt, where cavities along the edges where bubbles had formed are clearly visible, along with pedestal-like deposits of material that were likely at the bubble interface prior to depinning via the movement of the laser (Figure 3b).

Atomic force microscopy measurements showed that the height of the printed structures is only slightly influenced by these otherwise significant changes in microstructure, where the average height of Lap-EP is 109 ± 15.5 nm and that of Lap-RD is 93.7 ± 16.3 nm (Figure S1). The clear difference in the macroscopic appearance of the printed assemblies of pristine and organically modified Lap suggests that coating the layered silicate surface with different chemical groups could lead to drastic and interesting results. The use of molecules and

https://doi.org/10.1021/acsami.3c09760
ACS Appl. Mater. Interfaces 2023, 15, 55022−55029

polymers to modify the surface chemistry of nanoparticles printed by BP could be used to modulate the substrate–particle interactions, as well as adhesion and presumably the mechanical properties of the assembly, although this was outside the scope of this work.

Dye Loading and FRET-Based Sensing. Lap has been well established for its capability to adsorb dye molecules at the basal surface as well as by edge modification with dyes. Lap was modified with different cationic fluorescent Rhodamine dyes, and the printing was carried out as described above. The dye-loading capabilities of the bubble-printed layered silicates were maintained, as shown by absorption of several different fluorescent dyes (Figure S2a). BP was used to fabricate patterns composed of Lap with QDs of three different emission wavelengths interspersed among Lap, which showed fluorescence from the QDs (Figures 4 and S2b). Interestingly, the periodicity of the Lap-RD structure leads to a "strobe" light effect during printing due to the emission of the QDs at the bubble interface during printing (Video S4).

A proof-of-concept of the use of this technique for FRET-based sensors was carried out. FRET is mediated by dipole–dipole interactions of donor and acceptors, where instead of emitting and returning to its ground state, the energy of the donor fluorophore (QD) is nonradiatively transferred to the nearby acceptor fluorophore (R800).[53] Moreover, FRET only occurs when donor and acceptor molecules are very close to each other, typically within 10 nm, and the efficiency of energy transfer decreases as the distance between the two molecules increases beyond this range.[54] QDs with an emission of 620 nm could excite Rhodamine 800 (R800), which has an absorption band at 635 nm and an emission at 704 nm, via FRET. The detection sensitivity of R800 due to FRET from the QDs was assessed by measuring the fluorescence spectra of the printed patterns after soaking in R800 solutions from 1 pM to 1 μM (Figure 4a). First, quenching of the QD fluorescence was observed, even at R800 concentrations as low as 1 pM (Figure 4b). While this appears to be the limit of detection (LOD) for Lap-RD, the observed trend for Lap-EP suggests an even lower LOD. Next, the concomitant increase in R800 emission due to FRET from the QDs is observed, starting at R800 concentrations as low as 1 nM (Figure 4c). As observed by fluorescence microscopy, introduction of the fluorescent dye R800 decreased the QD emission (Figure 4d). While FRET between QDs and Rhodamine 6G has been shown,[55] the study of FRET between QDs and R800 had not been previously reported.

Interestingly, the hydrophobic Lap-EP showed drastically increased QD luminescence (~2.75×) compared to that of Lap-RD (Figure S3a). Furthermore, the intensity of the R800 peak due to FRET was also enhanced with Lap-EP compared to that with Lap-RD (Figures 4c and S3b). This relative increase of luminescence of both QD and dye is attributed to the hydrophobic environment of Lap-EP decreasing moisture-related quenching.[56] This established that the functional properties of both printed materials are maintained; the photoluminescence of the QDs (as previously reported[1]), and the layered silicate clays which enabled adsorption of organic dyes in aqueous solution. The bubble-printed FRET-based sensors with picomolar detection limit reported herein show the potential of assemblies of FRET donors with charged layered materials for detection applications due to the ability of the layered materials to adsorb analytes.

CONCLUSIONS

Herein, the printing of assemblies of pristine and organically modified Lap via a laser-driven microbubble was established. The printed patterns revealed clearly how the aggregation of particles at the bubble interface and periodic depinning of the bubble influenced the pattern morphology, whereas an increased speed of the laser movement led to "smeared" patterns with less defined interfacial boundaries. The printed patterns of pristine Lap-RD and organically modified Lap-EP drastically differed from one another, where Lap-EP assemblies minimized the interfacial contact with the liquid, which is energetically favorable. The ability of printed Lap-RD patterns to adsorb dye molecules was established with several Rhodamine dyes. Finally, both pristine and modified nanoclays were printed with QDs, providing fluorescent patterns that served as proof-of-concept FRET sensors with picomolar detection limits of R800. Interestingly, the observed fluorescence of patterns printed with Lap-EP was higher than for Lap-RD, suggesting that the hydrophobic nature of the modified clays can enhance their sensitivity.

The results of the FRET sensing experiments suggest that further avenues to exploit the adsorption of analytes should be sought. The potential to independently modify the basal surfaces noncovalently and the edge sites covalently provides many potential synthetic approaches to link biomolecules or other targets for selective sensing via several different modes of sensing.[57] The large detection range across concentrations down to picomolar levels can benefit a variety of target analytes. In addition to fluorescence quenching and FRET which was demonstrated with QDs, plasmonic metal nanoparticles could potentially provide plasmonic patterns to allow sensing by surface-enhanced Raman scattering.[20] Furthermore, organically modified nanoclays can template the colloidal growth of functional, semiconductor-based nanohybrids which retain many of the colloidal properties of layered silicates while also providing added functionality.[58−61] This class of materials represents a unique platform for introducing different functionalities, which could be easily and rapidly transferred to well-defined micropatterns via BP for myriad applications. The printed patterns are also robust and survived numerous cycles of washing under distilled water, drying under compressed air, and soaking for up to a combined 10 h in dye solutions of varying concentrations.

Overall, this work discloses the role of surface chemistry of anisotropic particles on assembly structure and underscores the potential of layered silicates as useful materials for multifunctional microscopic patterns with applications in sensing, devices, and lab-on-chip diagnostics, particularly environmental sensors, medical devices, and wearable electronics. These results show that particle self-assembly at the bubble interface, interactions with the vapor–liquid and liquid–substrate interfaces, and the resulting macroscopic structure and function of the printed material are all strongly related to surface chemistry at the particle interface. However, much is yet unknown about the relationship of surface chemistry, substrate, solvent, and particle morphology to these different parameters, beckoning further research. Future studies will seek to fill the gaps in knowledge of how the surface chemistry of anisotropic nanoparticles influences their hierarchical assembly at the interface.

https://doi.org/10.1021/acsami.3c09760
ACS Appl. Mater. Interfaces 2023, 15, 55022−55029

■ ASSOCIATED CONTENT

Supporting Information

The Supporting Information is available free of charge at https://pubs.acs.org/doi/10.1021/acsami.3c09760.

Atomic force microscopy height maps; fluorescence spectra of Lap-RD patterns and Lap-RD/QD hybrids; and non-normalized fluorescence emission spectra of Lap-QD micropatterns (PDF)

Video of pushing of "armored" bubbles formed in a dispersion of Lap-RD (MP4)

Video of BP of Lap-EP under brightfield illumination (MP4)

Video of BP of Lap-EP under dark-field illumination (MP4)

Video of BP of Lap-RD with 20 nM 625 nm QDs (MP4)

■ AUTHOR INFORMATION

Corresponding Authors

Eric H. Hill − *Institute of Physical Chemistry, University of Hamburg, 20146 Hamburg, Germany; The Hamburg Center for Ultrafast Imaging (CUI), 22761 Hamburg, Germany;* orcid.org/0000-0003-3063-1447; Email: eric.hill@chemie.uni-hamburg.de

Yuebing Zheng − *Materials Science & Engineering Program and Texas Materials Institute, The University of Texas at Austin, Austin, Texas 78712, United States; Walker Department of Mechanical Engineering, The University of Texas at Austin, Austin, Texas 78712, United States;* orcid.org/0000-0002-9168-9477; Email: zheng@austin.utexas.edu

Authors

Marcel Herber − *Institute of Physical Chemistry, University of Hamburg, 20146 Hamburg, Germany; The Hamburg Center for Ultrafast Imaging (CUI), 22761 Hamburg, Germany;* orcid.org/0000-0002-7097-1502

Ana Jiménez Amaya − *Institute of Physical Chemistry, University of Hamburg, 20146 Hamburg, Germany*

Nicklas Giese − *Institute of Physical Chemistry, University of Hamburg, 20146 Hamburg, Germany*

Bharath Bangalore Rajeeva − *Materials Science & Engineering Program and Texas Materials Institute, The University of Texas at Austin, Austin, Texas 78712, United States*

Complete contact information is available at: https://pubs.acs.org/10.1021/acsami.3c09760

Author Contributions

⊥M.H. and A.J.A. equal contribution

Notes

The authors declare no competing financial interest.

■ ACKNOWLEDGMENTS

This research was funded by the Deutsche Forschungsgemeinschaft (DFG)—project ID 447787198. E.H.H. and M.H. are supported by the Cluster of Excellence "Advanced Imaging of Matter" of the DFG—EXC 2056—project ID 390715994. N.G. acknowledges financial support by the DFG via the Research Training Group "Nanohybrid" (GRK 2536). Y.Z. acknowledges the financial support of the National Science Foundation (NSF-CMMI-1761743). We thank Professor William W. Yu for providing quantum dots.

■ REFERENCES

(1) Lin, L.; Peng, X.; Mao, Z.; Li, W.; Yogeesh, M. N.; Rajeeva, B. B.; Perillo, E. P.; Dunn, A. K.; Akinwande, D.; Zheng, Y. Bubble-Pen Lithography. *Nano Lett.* **2016**, *16* (1), 701−708.

(2) Kollipara, P. S.; Mahendra, R.; Li, J.; Zheng, Y. Bubble-Pen Lithography: Fundamentals and Applications. *Aggregate* **2022**, *3* (4), 1−16.

(3) Ghosh, S.; Ranjan, A. D.; Das, S.; Sen, R.; Roy, B.; Roy, S.; Banerjee, A. Directed Self-Assembly Driven Mesoscale Lithography Using Laser-Induced and Manipulated Microbubbles: Complex Architectures and Diverse Applications. *Nano Lett.* **2021**, *21* (1), 10−25.

(4) Xie, Y.; Zhao, C. An Optothermally Generated Surface Bubble and Its Applications. *Nanoscale* **2017**, *9* (20), 6622−6631.

(5) Baffou, G.; Polleux, J.; Rigneault, H.; Monneret, S. Super-Heating and Micro-Bubble Generation around Plasmonic Nanoparticles under Cw Illumination. *J. Phys. Chem. C* **2014**, *118* (9), 4890−4898.

(6) Baffou, G.; Quidant, R. Thermo-Plasmonics: Using Metallic Nanostructures as Nano-Sources of Heat. *Laser Photonics Rev.* **2013**, *7* (2), 171−187.

(7) Fang, Z.; Zhen, Y.-R.; Neumann, O.; Polman, A.; García de Abajo, F. J.; Nordlander, P.; Halas, N. J. Evolution of Light-Induced Vapor Generation at a Liquid-Immersed Metallic Nanoparticle. *Nano Lett.* **2013**, *13* (4), 1736−1742.

(8) Zhao, C.; Xie, Y.; Mao, Z.; Zhao, Y.; Rufo, J.; Yang, S.; Guo, F.; Mai, J. D.; Huang, T. J. Theory and Experiment on Particle Trapping and Manipulation via Optothermally Generated Bubbles. *Lab Chip* **2014**, *14* (2), 384−391.

(9) Zhao, C.; Liu, Y.; Zhao, Y.; Fang, N.; Jun Huang, T. A Reconfigurable Plasmofluidic Lens. *Nat. Commun.* **2013**, *4*, 2305.

(10) Meng, F.; Hao, W.; Yu, S.; Feng, R.; Liu, Y.; Yu, F.; Tao, P.; Shang, W.; Wu, J.; Song, C.; Deng, T. Vapor-Enabled Propulsion for Plasmonic Photothermal Motor at the Liquid/Air Interface. *J. Am. Chem. Soc.* **2017**, *139* (36), 12362−12365.

(11) Bangalore Rajeeva, B.; Lin, L.; Perillo, E. P.; Peng, X.; Yu, W. W.; Dunn, A. K.; Zheng, Y. High-Resolution Bubble Printing of Quantum Dots. *ACS Appl. Mater. Interfaces* **2017**, *9* (19), 16725−16733.

(12) Rajeeva, B. B.; Wu, Z.; Briggs, A.; Acharya, P. V.; Walker, S. B.; Peng, X.; Bahadur, V.; Bank, S. R.; Zheng, Y. "Point-and-Shoot" Synthesis of Metallic Ring Arrays and Surface-Enhanced Optical Spectroscopy. *Adv. Opt. Mater.* **2018**, *6* (10), 1701213.

(13) Rajeeva, B. B.; Kunal, P.; Kollipara, P. S.; Acharya, P. V.; Joe, M.; Ide, M. S.; Jarvis, K.; Liu, Y.; Bahadur, V.; Humphrey, S. M.; Zheng, Y. Accumulation-Driven Unified Spatiotemporal Synthesis and Structuring of Immiscible Metallic Nanoalloys. *Matter* **2019**, *1* (6), 1606−1617.

(14) Thomas, P.; Pei, C.; Roy, B.; Ghosh, S.; Das, S.; Banerjee, A.; Ben, T.; Qiu, S.; Roy, S. Site Specific Supramolecular Heterogeneous Catalysis by Optically Patterned Soft Oxometalate-Porous Organic Framework (SOM-POF) Hybrid on a Chip. *J. Mater. Chem. A* **2015**, *3* (4), 1431−1441.

(15) Armon, N.; Greenberg, E.; Layani, M.; Rosen, Y. S.; Magdassi, S.; Shpaisman, H. Continuous Nanoparticle Assembly by a Modulated Photo-Induced Microbubble for Fabrication of Micrometric Conductive Patterns. *ACS Appl. Mater. Interfaces* **2017**, *9* (50), 44214−44221.

(16) Edri, E.; Armon, N.; Greenberg, E.; Hadad, E.; Bockstaller, M. R.; Shpaisman, H. Assembly of Conductive Polyaniline Microstructures by a Laser-Induced Microbubble. *ACS Appl. Mater. Interfaces* **2020**, *12* (19), 22278−22286.

(17) Ghosh, S.; Das, S.; Paul, S.; Thomas, P.; Roy, B.; Mitra, P.; Roy, S.; Banerjee, A. In Situ Self-Assembly and Photopolymerization for Hetero-Phase Synthesis and Patterning of Conducting Materials

Using Soft Oxometalates in Thermo-Optical Tweezers. *J. Mater. Chem. C* **2017**, *5* (27), 6718−6728.
(18) Begley, M. R.; Gianola, D. S.; Ray, T. R. Bridging Functional Nanocomposites to Robust Macroscale Devices. *Science* **2019**, *364* (6447), No. eaav4299.
(19) Li, J.; Hill, E. H.; Lin, L.; Zheng, Y. Optical Nanoprinting of Colloidal Particles and Functional Structures. *ACS Nano* **2019**, *13* (4), 3783−3795.
(20) Hill, E. H.; Goldmann, C.; Hamon, C.; Herber, M. Laser-Driven Bubble Printing of Plasmonic Nanoparticle Assemblies onto Nonplasmonic Substrates. *J. Phys. Chem. C* **2022**, *126* (17), 7622−7629.
(21) Herber, M.; Lengle, D.; Valandro, S. R.; Wehrmeister, M.; Hill, E. H. Bubble Printing of $Ti_3C_2T_X$ MXene for Patterning Conductive and Plasmonic Nanostructures. *Nano Lett.* **2023**, *23* (14), 6308−6314.
(22) Suman, K.; Joshi, Y. M. Microstructure and Soft Glassy Dynamics of an Aqueous Laponite Dispersion. *Langmuir* **2018**, *34*, 13079−13103.
(23) López Arbeloa, F.; Martínez Martínez, V. Orientation of Adsorbed Dyes in the Interlayer Space of Clays. 2 Fluorescence Polarization of Rhodamine 6G in Laponite Films. *Chem. Mater.* **2006**, *18* (6), 1407−1416.
(24) Salleres, S.; López Arbeloa, F.; Martínez Martínez, V.; Arbeloa, T.; López Arbeloa, I. On the Arrangements of R6G Molecules in Organophilic C12TMA/Lap Clay Films for Low Dye Loadings. *Langmuir* **2010**, *26* (2), 930−937.
(25) Greathouse, J. A.; Geatches, D. L.; Pike, D. Q.; Greenwell, H. C.; Johnston, C. T.; Wilcox, J.; Cygan, R. T. Methylene Blue Adsorption on the Basal Surfaces of Kaolinite: Structure and Thermodynamics from Quantum and Classical Molecular Simulation. *Clays Clay Miner.* **2015**, *63* (3), 185−198.
(26) Cenens, J.; Schoonheydt, R. A. Visible Spectroscopy of Methylene Blue on Hectorite, Laponite B, and Barasym in Aqueous Suspension. *Clays Clay Miner.* **1988**, *36* (3), 214−224.
(27) Hill, E. H.; Zhang, Y.; Whitten, D. G. Aggregation of Cationic P-Phenylene Ethynylenes on Laponite Clay in Aqueous Dispersions and Solid Films. *J. Colloid Interface Sci.* **2015**, *449*, 347−356.
(28) Schoonheydt, R. A. Functional Hybrid Clay Mineral Films. *Appl. Clay Sci.* **2014**, *96*, 9−21.
(29) Belušáková, S.; Lang, K.; Bujdák, J. Hybrid Systems Based on Layered Silicate and Organic Dyes for Cascade Energy Transfer. *J. Phys. Chem. C* **2015**, *119* (38), 21784−21794.
(30) Wheeler, P. A.; Wang, J.; Baker, J.; Mathias, L. J. Synthesis and Characterization of Covalently Functionalized Laponite Clay. *Chem. Mater.* **2005**, *17* (11), 3012−3018.
(31) Felbeck, T.; Hoffmann, K.; Lezhnina, M. M.; Kynast, U. H.; Resch-Genger, U. Fluorescent Nanoclays—Covalent Functionalization with Amine Reactive Dyes from Different Fluorophore Classes and Surface Group Quantification. *J. Phys. Chem. C* **2015**, *119*, 12978−12987.
(32) Kaup, G.; Felbeck, T.; Staniford, M.; Kynast, U. Towards the Rare Earth Functionalization of Nano-Clays with Luminescent Reporters for Biophotonics. *J. Lumin.* **2016**, *169*, 581−586.
(33) Xiang, H.; Valandro, S. R.; Hill, E. H. Layered Silicate Edge-Linked Perylene Diimides : Synthesis, Self-Assembly and Energy Transfer. *J. Colloid Interface Sci.* **2023**, *629*, 300−306.
(34) Lotsch, B. V.; Ozin, G. A. Photonic Clays: A New Family of Functional 1D Photonic Crystals. *ACS Nano* **2008**, *2* (10), 2065−2074.
(35) Fan, Q.; Shan, D.; Xue, H.; He, Y.; Cosnier, S. Amperometric Phenol Biosensor Based on Laponite Clay-Chitosan Nanocomposite Matrix. *Biosens. Bioelectron.* **2007**, *22* (6), 816−821.
(36) Senillou, A.; Jaffrezic, N.; Martelet, C.; Cosnier, S. A Laponite Clay-Poly(Pyrrole-Pyridinium) Matrix for the Fabrication of Conductimetric Microbiosensors. *Anal. Chim. Acta* **1999**, *401* (1−2), 117−124.
(37) Vaiana, C. A.; Leonard, M. K.; Drummy, L. F.; Singh, K. M.; Bubulya, A.; Vaia, R. A.; Naik, R. R.; Kadakia, M. P. Epidermal Growth Factor: Layered Silicate Nanocomposites for Tissue Regeneration. *Biomacromolecules* **2011**, *12* (9), 3139−3146.
(38) Eslahi, N.; Simchi, A.; Mehrjoo, M.; Shokrgozar, M. A.; Bonakdar, S. Hybrid Cross-Linked Hydrogels Based on Fibrous Protein/Block Copolymers and Layered Silicate Nanoparticles: Tunable Thermosensitivity, Biodegradability and Mechanical Durability. *RSC Adv.* **2016**, *6* (67), 62944−62957.
(39) Ghadiri, M.; Chrzanowski, W.; Lee, W. H.; Rohanizadeh, R. Layered Silicate Clay Functionalized with Amino Acids: Wound Healing Application. *RSC Adv.* **2014**, *4* (67), 35332−35343.
(40) Mousa, M.; Evans, N. D.; Oreffo, R. O. C.; Dawson, J. I. Clay Nanoparticles for Regenerative Medicine and Biomaterial Design: A Review of Clay Bioactivity. *Biomaterials* **2018**, *159* (2018), 204−214.
(41) Dawson, J. I.; Oreffo, R. O. C. Clay: New Opportunities for Tissue Regeneration and Biomaterial Design. *Adv. Mater.* **2013**, *25* (30), 4069−4086.
(42) Han, L.; Lu, X.; Liu, K.; Wang, K.; Fang, L.; Weng, L. T.; Zhang, H.; Tang, Y.; Ren, F.; Zhao, C.; Sun, G.; Liang, R.; Li, Z. Mussel-Inspired Adhesive and Tough Hydrogel Based on Nanoclay Confined Dopamine Polymerization. *ACS Nano* **2017**, *11* (3), 2561−2574.
(43) Ahlfeld, T.; Cidonio, G.; Kilian, D.; Duin, S.; Akkineni, A. R.; Dawson, J. I.; Yang, S.; Lode, A.; Oreffo, R. O. C.; Gelinsky, M. Development of a Clay Based Bioink for 3D Cell Printing for Skeletal Application. *Biofabrication* **2017**, *9* (3), 034103.
(44) Tu, H.; Dai, F.; Cheng, G.; Yuan, M.; Zhou, X.; Wang, Y.; Zhang, R.; Zheng, Y.; Cheng, Y.; Deng, H. Incorporation of Layered Rectorite into Biocompatible Core-Sheath Nanofibrous Mats for Sustained Drug Delivery. *ACS Biomater. Sci. Eng.* **2021**, *7* (9), 4509−4520.
(45) Jayrajsinh, S.; Shankar, G.; Agrawal, Y. K.; Bakre, L. Montmorillonite Nanoclay as a Multifaceted Drug-Delivery Carrier: A Review. *J. Drug Delivery Sci. Technol.* **2017**, *39*, 200−209.
(46) Jafarbeglou, M.; Abdouss, M.; Shoushtari, A. M.; Jafarbeglou, M. Clay Nanocomposites as Engineered Drug Delivery Systems. *RSC Adv.* **2016**, *6* (55), 50002−50016.
(47) Yu, W. W.; Chang, E.; Falkner, J. C.; Zhang, J.; Al-Somali, A. M.; Sayes, C. M.; Johns, J.; Drezek, R.; Colvin, V. L. Forming Biocompatible and Nonaggregated Nanocrystals in Water Using Amphiphilic Polymers. *J. Am. Chem. Soc.* **2007**, *129* (10), 2871−2879.
(48) Yu, W. W.; Qu, L.; Guo, W.; Peng, X. Experimental Determination of the Extinction Coefficient of CdTe, CdSe and CdS Nanocrystals. *Chem. Mater.* **2004**, *16* (3), 560.
(49) Liu, Q.; Zhang, S.; Sun, D.; Xu, J. Aqueous Foams Stabilized by Hexylamine-Modified Laponite Particles. *Colloids Surf., A* **2009**, *338* (1−3), 40−46.
(50) Zhang, S.; Lan, Q.; Liu, Q.; Xu, J.; Sun, D. Aqueous Foams Stabilized by Laponite and CTAB. *Colloids Surf., A* **2008**, *317* (1−3), 406−413.
(51) Cui, Y.; Kumar, S.; Rao Kona, B.; Van Houcke, D. Gas Barrier Properties of Polymer/Clay Nanocomposites. *RSC Adv.* **2015**, *5* (78), 63669−63690.
(52) Lin, L.; Peng, X.; Wei, X.; Mao, Z.; Xie, C.; Zheng, Y. Thermophoretic Tweezers for Low-Power and Versatile Manipulation of Biological Cells. *ACS Nano* **2017**, *11* (3), 3147−3154.
(53) Forster, T. Intermolecular Energy Transfer and Fluorescence. *Ann. Phys. Leipzig* **1948**, *2*, 55−75.
(54) Morgner, F.; Geißler, D.; Stufler, S.; Butlin, N. G.; Löhmannsröben, H.; Hildebrandt, N. A Quantum-Dot-Based Molecular Ruler for Multiplexed Optical Analysis. *Angew. Chem., Int. Ed.* **2010**, *49* (41), 7570−7574.
(55) Bharadwaj, K.; Koley, S.; Jana, S.; Ghosh, S. Model-Free Estimation of Energy-Transfer Timescales in a Closely Emitting CdSe/ZnS Quantum Dot and Rhodamine 6G FRET Couple. *Chem. - Asian J.* **2018**, *13* (21), 3296−3303.
(56) Maillard, J.; Klehs, K.; Rumble, C.; Vauthey, E.; Heilemann, M.; Fürstenberg, A. Universal Quenching of Common Fluorescent Probes by Water and Alcohols. *Chem. Sci.* **2021**, *12* (4), 1352−1362.

(57) Xiang, H.; Valandro, S. R.; Hill, E. H. 2D Nanomaterial-Directed Molecular Aggregation and Energy Transfer between Edge-Bound Donor-Acceptor Pairs. *J. Phys. Chem. C* **2023**, *127* (31), 15416−15422.
(58) Jatav, S.; Furlan, K. P.; Liu, J.; Hill, E. H. Heterostructured Monolayer MoS_2 Nanoparticles toward Water-Dispersible Catalysts. *ACS Appl. Mater. Interfaces* **2020**, *12* (17), 19813−19822.
(59) Liu, J.; Jatav, S.; Hill, E. H. Few-Layer In_2S_3 in Laponite Interlayers: A Colloidal Route Toward Heterostructured Nanohybrids with Enhanced Photocatalysis. *Chem. Mater.* **2020**, *32* (23), 10015−10024.
(60) Liu, J.; Jatav, S.; Wessel, P.; Hill, E. H. Templating Unidirectional Bismuth Oxyiodide Crystal Growth with Layered Silicates for Enhanced Photocatalysis. *J. Phys. Chem. C* **2022**, *126* (10), 4975−4983.
(61) Liu, J.; Jatav, S.; Herber, M.; Hill, E. H. Few-Layer $ZnIn_2S_4$/Laponite Heterostructures: Role of Mg^{2+} Leaching in Zn Defect Formation. *Langmuir* **2021**, *37* (15), 4727−4735.

https://doi.org/10.1021/acsami.3c09760
ACS Appl. Mater. Interfaces 2023, 15, 55022−55029